Fast and Robust Single-Phase DQ Current Controller for Smart Inverter Applications

Mohammad Ebrahimi, *Student Member, IEEE*, Sayed Ali Khajehoddin, *Member, IEEE*, and Masoud Karimi-Ghartemani, *Senior Member, IEEE*

***Abstract*—This paper presents a fast and robust DQ current controller to regulate the output power of single-phase grid-connected inverters. The proposed method generates the grid current orthogonal component without introducing any additional dynamics or distortions to the control loop. Moreover, its operation does not depend on the system parameters. The proposed method exhibits improved steady-state and dynamic performances in comparison with the inverters equipped with the conventional orthogonal signal generation techniques. Its improved characteristics make the proposed controller suitable for smart inverter applications, to provide advanced grid functionalities as demanded by recently revised standards. Simulation and experimental results show the feasibility and performance of this control structure.**

***Index Terms*—Advanced grid functionality (AGF), current control, DQ frame, low-voltage ride through (LVRT), orthogonal signal generation (OSG), single-phase grid-connected inverter.**

I. Introduction

DUE to the growing penetration of distributed generation (DG) units into the power grid, standards in many countries are recently amended, requiring DGs to provide advanced grid functionality (AGF). These functionalities aim to support the grid during faults and fluctuations. Low-/high-voltage ride through (L/HVRT), low-/high-frequency ride through (L/HFRT), and reactive power generation are examples of the AGFs expected by the revised standards [1]–[5].

Realization of such functionalities in the DG needs an advanced control structure. Since the inverter plays the key role in control of the DG, its controller is expected to be designed adequately to help the DG comply with the new standards. Accordingly, as the basic requirement, an advanced and smart inverter needs fast and robust dynamics with flexible control structure that is able to regulate its output power in all operating conditions of the grid.

Two common methods for power regulation of the smart inverter are: 1) using proportional-resonant (PR) controllers in stationary reference frame or equally $\alpha\beta$ frame, and 2) transforming the variables to synchronous reference frame (SRF) or equally DQ frame, and using proportional-integral (PI) controllers. PR controllers in stationary frame are simple, and they can control either the instantaneous power of the inverter directly [6], or the average value of the output power by means of the conventional current control schemes. The PI controller in SRF is also a well-known structure, providing power regulation based on the instantaneous power theory [7], [8]. PR controllers in $\alpha\beta$ frame are basically equivalent (in view of the fundamental frequency) to PI controllers in DQ frame [9]. Depending on the application, either of these methods is used. In this study, a DQ frame controller is applied to the smart inverter to provide a fast and robust power regulation scheme.

DQ frame controllers were originally introduced for three-phase systems, and then, extended to single-phase applications [10]. In these controllers, $\alpha\beta/DQ$ transformation turns ac variables into equivalent dc quantities, thus they can be controlled by PI controllers. The design process of PI controllers is simple and they exhibit satisfactory dynamic and steady-state performance. Also, as the system variables are converted to dc quantities, the control loop has no dependence on the system frequency. In addition, this scheme can regulate active and reactive power independently by simple adjustment of the D and Q-axis currents, respectively.

DQ current control of single-phase inverters requires an orthogonal signal generation (OSG) block to provide the orthogonal component of the grid current in $\alpha\beta$ frame [10]–[12]. Conventionally, OSG is implemented using phase shift methods such as Hilbert transform [13]–[15], time delay [11], [16], all pass filter [17], [18], and second-order generalized integrator (SOGI) [19]. Although the steady-state performance of these methods are acceptable for most part, the delay to create 90ºphase shift slows down the system dynamic response that can be problematic in smart inverters. Moreover, frequency drifts result in an inaccurate phase shift, which could lead to unacceptable errors in active and reactive power control.

Some methods are proposed to eliminate the undesired phase shift block in the control system. In one approach, the grid side filter capacitor current and its voltage are used because of their inherent 90º phase difference [10]. This method has several drawbacks. First, the measured capacitor current contains large amount of switching harmonics, which can degrade the current controller performance. Furthermore, this method is only applicable to inverters that use *LC* or *LCL* output filters. Accordingly, in case of the *LCL* filter, if the capacitor current and grid voltage are used, they would not have exact 90º phase shift, resulting in steady-state error in DQ currents. In another approach, the fictive axis emulation (FAE) [20], the orthogonal component of

Manuscript received February 2, 2015; revised June 3, 2015; accepted August 16, 2015. Date of publication August 11, 2015; date of current version December 10, 2015. Recommended for publication by Associate Editor K.-B. Lee.

M. Ebrahimi and S. A. Khajehoddin are with the Department of Electrical and Computer Engineering, University of Alberta, Edmonton, AB T6G 1H9 Canada (e-mail: eb2@ualberta.ca; khajeddin@ualberta.ca).

M. Karimi-Ghartemani is with the Department of Electrical and Computer Engineering, Mississippi State University, Starkville, MS 39762 USA (e-mail: karimi@ece.msstate.edu).

Color versions of one or more of the figures in this paper are available online at http://ieeexplore.ieee.org.

Digital Object Identifier 10.1109/TPEL.2015.2474696

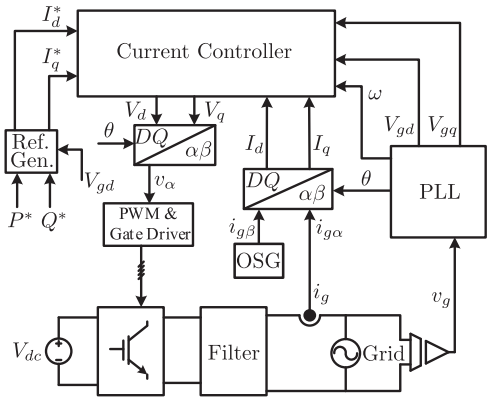

Fig. 1. Block diagram of DQ controlled single-phase grid-connected inverter.

the grid current is generated by virtually emulating the output filter inductor in the controller. Although this method is simple and successfully generates the orthogonal component for an inverter with inductive output filter, it is a model-based approach and its performance and response depend on the system parameters that may be uncertain and/or prone to change. In addition, the implementation of this method for an inverter using the *LCL* output filter has not been studied in the literature.

In this paper, a new OSG method is proposed that makes the controller independent of the system parameters and operating frequency. Moreover, the method is instantaneous and does not introduce any additional delay, nor any distortion to the control process. This method shows superior dynamic performance compared with the conventional single-phase DQ current controllers. The enhanced dynamic performance along with the ability of the DQ controller for instantaneous power control (IPC), make the proposed control scheme a suitable choice for power regulation of the smart inverters. Accordingly, performance of the proposed method is further investigated for the LVRT feature as an example of an AGF, which helps increase the grid stability.

This paper is organized as follows. Overall system and the proposed method are described in Section II. Section III presents the detailed description of the LVRT feature. In Section IV, performance evaluation and comparison with other methods are presented. Finally, the paper is concluded in Section V.

II. Proposed Method

A general block diagram of a single-phase grid-connected inverter controlled in DQ frame is shown in Fig. 1, where the inverter is interfaced with the grid through a passive filter. Grid voltage and the current are fed back to the controller. The controller is responsible for injecting a sinusoidal current meeting the grids' requirements on power quality and dynamic performance. As it can be seen in this figure, current controller needs an OSG block to generate the β-axis component of the grid current ($i_{g\beta}$). In addition, a phase-locked loop (PLL) is used in this scheme to synchronize the inverter to the grid.

Details of the DQ frame current controller is shown in Fig. 2. This controller consists of PI controllers, decoupling terms, and

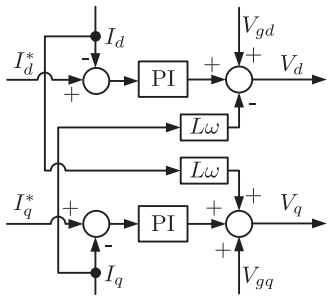

Fig. 2. Block diagram of the current controller in DQ frame.

feed-forward terms in both D- and Q-axes. This structure is same as the three-phase DQ frame current controllers [21].

A. Proposed OSG Technique

Assuming the grid current as (1), the 90º delayed version of this current will have the form of (2)

$$i_{g\alpha} = A\sin(\theta+\varphi) \tag{1}$$

$$i_{g\beta} = -A\cos(\theta+\varphi) \tag{2}$$

where

$$\theta = \int_0^t \omega(\tau)d\tau. \tag{3}$$

In (1)–(3), ω and θ are the angular frequency and phase angle of the grid voltage, and φ is the phase angle between the grid voltage and current.

The reference value of the D- and Q-axes currents (I_d^* and I_q^*) correspond to α-axis reference current ($i_{g\alpha}^*$) in the form of

$$i_{g\alpha}^* = B\sin(\psi+\gamma) \tag{4}$$

where ψ is angle of the $\alpha\beta/DQ$ transformation and

$$B = \sqrt{I_d^{*2}+I_q^{*2}} \quad , \quad \gamma = \tan^{-1}\left(\frac{I_q^*}{I_d^*}\right). \tag{5}$$

The objective is to estimate the actual $i_{g\beta}$. If the PLL is operating in steady state, ψ will be equal to θ. Meanwhile, since PI controllers are chosen and they eliminate the steady-state error of the current controller, $i_{g\alpha}$ will eventually become equal to $i_{g\alpha}^*$. Similarly, if the β-axis component of the grid current actually existed, this current also would have become equal to $i_{g\beta}^*$. Therefore, the β-axis component can be estimated based on the reference value of the D- and Q-axes currents. In view of that, the proposed method uses I_d^* and I_q^* values to generate an estimation of $i_{g\beta}$ (i.e., $\hat{i}_{g\beta}$) in the form of (6). A block diagram of this method is shown in Fig. 3

$$\hat{i}_{g\beta} = -B\cos(\psi+\gamma). \tag{6}$$

The proposed method does not introduce any dynamics in generating the orthogonal signal and does not introduce any distortion into it. Therefore, it results in a fast and smooth output current response. In addition, this method has no dependence on the systems' model (such as the inductance), since the β-axis

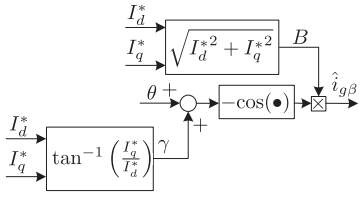

Fig. 3. Block diagram of the proposed OSG technique.

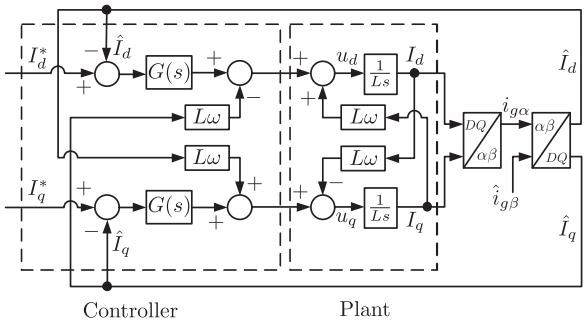

Fig. 4. Block diagram of the controller and plant in DQ frame using the proposed method as the OSG. The grid-side filter is assumed to be an inductor.

current is generated solely based on the reference values of the D- and Q-axis currents.

B. Stability Analysis of Proposed Control System

Fig. 4 shows the representation of the controller and plant in DQ frame. This system uses an inductor as the grid-side filter. Since it is assumed that the actual grid voltage and its related feed forward term in the controller perfectly cancel each other, these two terms are not shown in this figure. The filter current is transformed to DQ frame, hence, the output current is obtained in D- and Q-axes, i.e., I_d and I_q. The grid current in β-axis is not available and the proposed method is used for estimating it according to (6). The $\alpha\beta/DQ$ transformation of this current along with the actual grid current in α axis provides an estimation of grid current in D- and Q-axes, which is denoted by $\hat{I}_d$ and $\hat{I}_q$ and can be represented as

$$\overrightarrow{\hat{I}_{dq}}(t) = \begin{bmatrix} \sin(\theta) & -\cos(\theta) \\ \cos(\theta) & \sin(\theta) \end{bmatrix} \begin{bmatrix} i_{g\alpha}(t) \\ \hat{i}_{g\beta}(t) \end{bmatrix}. \tag{7}$$

Substituting $[\, i_{g\alpha}(t) \quad \hat{i}_{g\beta}(t)\,]^T$ by its DQ frame representation results in

$$\begin{aligned} \hat{I}_d(t) &= \frac{I_d}{2} + \frac{I_d^*}{2} + \frac{I_q - I_q^*}{2}\sin(2\theta) - \frac{I_d - I_d^*}{2}\cos(2\theta) \\ \hat{I}_q(t) &= \frac{I_q}{2} + \frac{I_q^*}{2} + \frac{I_d - I_d^*}{2}\sin(2\theta) + \frac{I_q - I_q^*}{2}\cos(2\theta). \end{aligned} \tag{8}$$

Note that the double-frequency terms of (8) go to zero if I_d and I_q approach I_d^* and I_q^*, respectively. Equation (8) indicates that this system can be represented as a linear time-varying system with a combination of an LTI system and a system with double-frequency dynamics. The closed-loop stability of the system can be analyzed using the two time-scale method. Extensive simulation studies and experimental results confirm that the

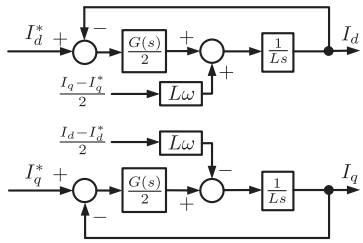

Fig. 5. Block diagram of the system for stability analysis.

double-frequency subsystem does not have any destabilizing impact on the LTI subsystem. Thus, ignoring the double-frequency terms, (8) becomes

$$\overrightarrow{\hat{I}_{dq}}(t) - \overrightarrow{I_{dq}^*} = \frac{1}{2}\left(\overrightarrow{I_{dq}} - \overrightarrow{I_{dq}^*}\right). \tag{9}$$

Block diagram of system in Fig. 4 is redrawn as depicted in Fig. 5. In this block diagram, $\hat{I}_d(t)$ and $\hat{I}_q(t)$ are substituted according to (9). Also the PI controllers are shown as $G(s)$, where $G(s) = (k_p s + k_i)/s$.

The reference values in disturbance inputs of Fig. 5 will be removed by the PI controllers, hence they can be ignored. So, this system can be represented as

$$\begin{bmatrix} I_d(s) \\ I_q(s) \end{bmatrix} = \frac{G(s)}{G(s)+2Ls} \begin{bmatrix} 1 & -\dfrac{L\omega}{G(s)+2Ls} \\ \dfrac{L\omega}{G(s)+2Ls} & 1 \end{bmatrix}^{-1} \times \begin{bmatrix} I_d^*(s) \\ I_q^*(s) \end{bmatrix}. \tag{10}$$

The inverse matrix in (10) is calculated and $I_d^*(s)$ and $I_q^*(s)$ are considered as step functions in the form of (11)

$$\begin{aligned} I_d^*(s) &= \frac{I_d^{\text{ref}}}{s} \\ I_q^*(s) &= \frac{I_q^{\text{ref}}}{s}. \end{aligned} \tag{11}$$

Considering (10) and (11), and using the final value theorem (FVT), it can be concluded that

$$\begin{aligned} \lim_{t\to\infty} I_d(t) &= \lim_{s\to 0} sI_d(s) = I_d^{\text{ref}} \\ \lim_{t\to\infty} I_q(t) &= \lim_{s\to 0} sI_q(s) = I_q^{\text{ref}}. \end{aligned} \tag{12}$$

Therefore, the whole system is stable and D and Q-axes currents approach to their set point values. The sole condition for the stability is the same as the condition for the applicability of the FVT and that is the roots of $G(s) + 2Ls$ should be stable. This condition is satisfied for all positive k_p and k_i.

C. PI Controller Design

PI controllers for both D- and Q-axes are designed based on the systems' model. According Fig. 4 and assuming a non-ideal inductor filter as the plant (i.e., $\frac{I_d}{u_d} = \frac{I_q}{u_q} = \frac{1}{Ls+R}$), the

open-loop transfer function of the system will be equal to

$$l(s) = \frac{k_p}{Ls}\left(\frac{s + k_i/k_p}{s + R/L}\right). \tag{13}$$

In (13), the plant pole ($s = -R/L$) can be canceled by the compensator zero ($s = -k_i/k_p$) by choosing k_p and k_i as $k_p = L/\tau_i$ and $k_i = R/\tau_i$. As a result, the closed-loop transfer function of the system will be equal to

$$G(s) = \frac{I_d(s)}{I_d^{\text{ref}}(s)} = \frac{I_q(s)}{I_q^{\text{ref}}(s)} = \frac{1}{\tau_i s + 1} \tag{14}$$

where τ_i (time constant of the closed-loop system) is a design parameter [21]. Using this procedure, PI controllers can be designed for both D- and Q-axes.

In addition, sensitivity of the PI controllers to the inductor value variations can be assessed based on (13). In this regard, time constant of the output response (i.e., $I_d(s)$ or $I_q(s)$) is taken into account. Considering (13), it is noted that this parameter in both D- and Q-axes is dominantly characterized by the term $\frac{L}{k_p}$. Therefore, any inductor detunings causes the time constant to deviate from its designed value.

III. LVRT Feature

A. LVRT Description

As the number of integrated renewable DG units in a power grid increases, simultaneous disconnection of all DGs in case of a voltage sag can result further system instability and power quality issues. Therefore, new regulations obligate the smart inverters to support the grid by providing a specified amount of reactive power in case of voltage sag [22], [23]. This is called LVRT feature.

The allowable off-grid and grid-connected regions of a DG system is determined by the grid codes of each country. The grid-connected region is defined based on depth and duration of the sag. In some countries such as Italy and Germany, there are even a short time interval (100∼150 ms) with zero-volt grid voltage that the DG has to remain connected to the grid [22]. The short time intervals provided by the grid codes, require fast dynamic response controllers such as the one proposed in this paper.

In a DQ frame current controlled inverter, both active and reactive powers can be controlled independently. This can be employed to introduce the LVRT feature to a single-phase DG unit. In normal operating condition, the D-axis reference current (I_d^*) is adjusted based on the reference value of the active power. Also the arbitrary level of reactive power determines the reference of the Q-axis current (I_q^*). In a grid fault situation, however, I_q^* will be adjusted based on the depth of the voltage sag, according to the standard. Several approaches have been proposed to determine I_d^* in case of a voltage sag. Constant peak current, constant active current, and constant average active power strategies are such examples [22], [23]. Among these strategies, only the constant peak current strategy dictates the amount of active current with taking the inverters' maximum current capacity into consideration. In this strategy, I_d^* is calculated based on

$$I_d^* = \sqrt{{I_{g\max}}^2 - {I_q^*}^2} \tag{15}$$

where $I_{g\max}$ is the peak value of the inverters' maximum current without tripping the over current protection.

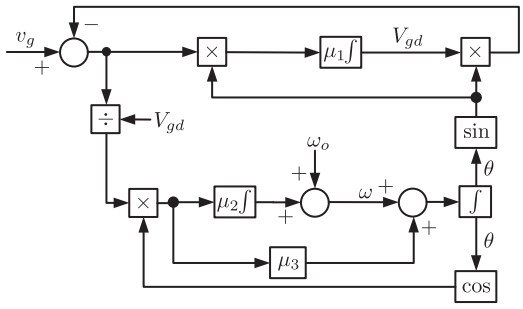

Fig. 6. Block diagram of the PL-EPLL.

B. Fault Detection

As the voltage sag fault occurs, it should be rapidly detected to trigger the LVRT function in the controller for adjustment of active and reactive power reference values. Detection of fault condition can be done through monitoring of estimated grid voltage amplitude at the PLL output. Based on this scenario, this system needs a fast and robust PLL technique. This PLL has to be accurate for different grid voltage frequency and amplitudes.

Enhanced PLL (EPLL) has been widely used in single-phase grid-connected applications [24]. The EPLL, however, depends on the input signal magnitude while the LVRT needs a scheme that can work for small or even zero-grid voltage condition. The pseudolinear-EPLL (PL-EPLL) is recently proposed that has a fast response and works for all input magnitudes [25]. The PL-EPLL provides the grid voltage amplitude that can be utilized to detect the fault condition. Moreover, the PL-EPLL is capable of producing a synchronization signal even if grid voltage is reduced to about zero as this signal is necessary for the controller to inject the required reactive current under such circumstances. Block diagram of the PL-EPLL is shown in Fig. 6.

IV. Simulation and Experimental Results

The proposed control method is tested and its steady-state and dynamic performances are evaluated using simulations and laboratory experiments. The results are also compared to conventional OSG techniques. System parameters are listed in Table I.

A. Dynamic and Steady-State Performance Evaluation

Basic dynamic performance of the proposed method is evaluated in a scenario where the inverter is first injecting zero active and reactive power. At $t = 0.104$ s, P^* changes to 600 W and after that at $t = 0.13$ s, Q^* changes to 450 VAR. Results are shown in Fig. 7. It is observed that the proposed method presents a fast dynamic response and tracks the step change in the current reference values with no steady error.

TABLE I
SYSTEM PARAMETERS

Dc link voltage		200	V
Grid voltage		120	V
Grid frequency		60	Hz
Grid side filter inductance		12	mH
Switching frequency		10	kHz
Sampling frequency		5	kHz
PI controller gains	Prop.(K_p)	40	
	Integ. (K_i)	500	
PL-EPLL gains	μ_1, μ_3	500	
	μ_2	3500	

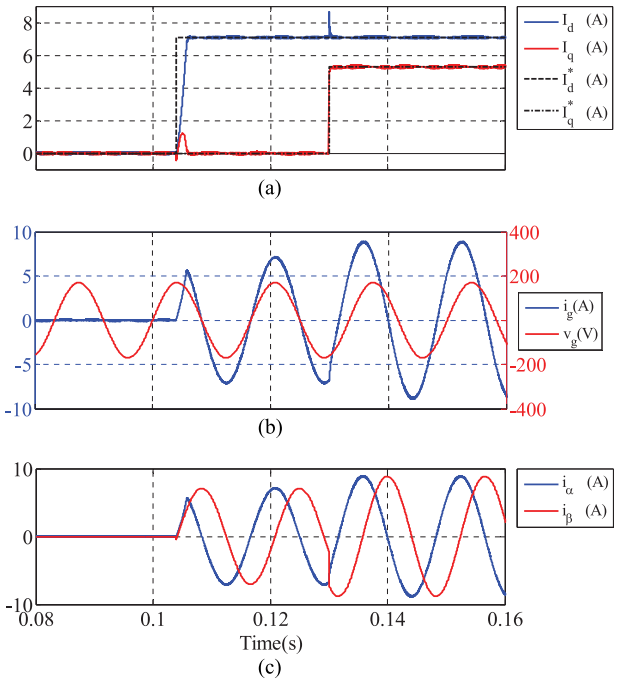

Fig. 7. Dynamic performance evaluation of the proposed method. P^* changes from zero to 600 W at $t = 0.104$ s and Q^* from zero to 450 VAR at $t = 0.13$ s. (a) Grid current in both D- and Q-axes along with their reference values. (b) Grid current and voltage. (c) Grid current in α- and β-axes.

The steady-state performance of the method in the presence of 10% third harmonic in grid voltage is evaluated in the following simulation. P^* and Q^* has been set to 600 W and 0 VAR, respectively. The variables I_d and I_q and their reference values are shown in Fig. 8(a). Fig. 8(b) shows the injected current and the grid voltage. Although the grid voltage is unrealistically polluted with 10% of the third harmonic, inverter is still injecting a highly sinusoidal current with total harmonic distortion (THD) equal to 2.47%. The harmonic spectrum of the grid current is also shown in Fig. 8(c).

Performance of the proposed method is compared with different OSG techniques and the results are presented in Fig. 9. The conventional methods in this study are introduced in Table II. This test confirms superior performance of the proposed method in comparison with the conventional delay- and phase shift-based techniques. It can be observed from Fig. 9 that the performance of the proposed method is similar to the FAE

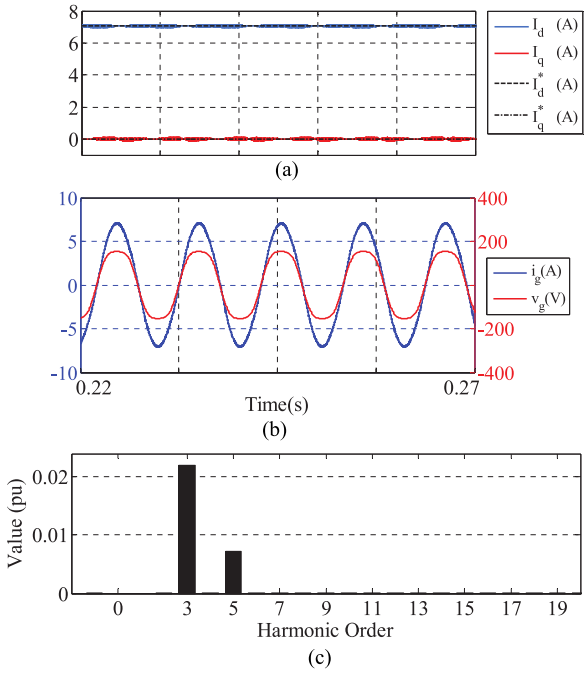

Fig. 8. Results for the steady-state performance of the proposed method in the presence of 10% third harmonic in the grid voltage. (a) Grid current in both D- and Q-axis along with their reference values. (b) Grid current and voltage. (c) Harmonic spectrum of the grid current.

method. The reason is that regardless of the actual grid current in α-axis, both methods virtually generate the orthogonal component of the grid current with no delay. The FAE performance, however, depends on system parameters because the FAE method generates the orthogonal component using a virtual filter that is implemented in the controller and needs the inductance value. The proposed method in this paper has the advantage that the orthogonal current generation system is independent from the system parameters. The sensitivity of FAE is tested by doubling the inductance of the virtual filter. In this test, the actual grid filter inductance is 12 mH, while the FAE is implemented with 24mH inductance. Fig. 10 shows the results obtained from both proposed and FAE methods. As it can be seen in this figure, a mismatch between the actual and the virtual filter inductance, leads to some sustained oscillations in the D- and Q-axes currents and also degrades tracking performance of the FAE method.

B. LCL Filter

Both FAE and the proposed method are tested in a system using an *LCL* filter and results are shown in Fig. 11. As it can be observed in this figure, proposed method perfectly works for the *LCL* filter as well. Utilization of the FAE method in this system, however, generates some sustained oscillations in DQ currents. The reason is that FAE is designed for the *L* filter, and its application in higher order filters like LCL needs modifications. These modifications, however, make this method too complicated. In addition, the FAE method makes the current controller dependent on the filter parameters, and an *LCL* filter, makes the FAE dependent on three different parameters of the

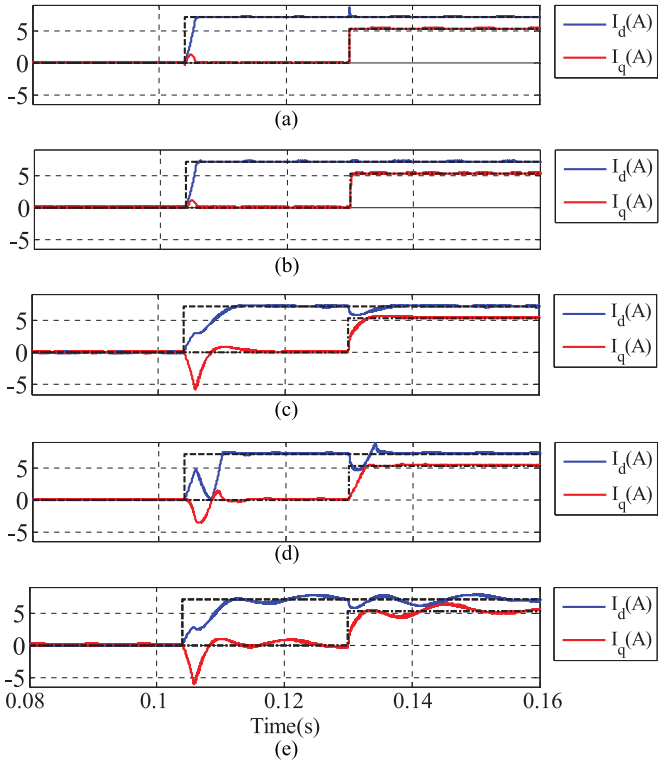

Fig. 9. Dynamic performance comparison of different OSG techniques. (a) Proposed method. (b) FAE [20]. (c) Hilbert transform [14], [15]. (d) Time delay [11]. (e) Second-order all pass filter [17], [18]. In this test P^* changes from zero to 600 W at $t = 0.104$ s and Q^* from zero to 450 VAR at $t = 0.13$ s.

TABLE II
TRANSFER FUNCTION OF THE CONVENTIONAL OSG TECHNIQUES

Hilbert transform [14], [15]	Second order all pass filter [17], [18]
$G(s) = \frac{\omega_b - s}{\omega_b + s}$	$G(s) = \frac{-(s^2 - 2\omega_n s + \omega_n^2)}{s^2 + 2\omega_n s + \omega_n^2}$

ω_b: Grid angular frequency.
$\omega_n = (\sqrt{2} - 1)\,\omega_b$.

system. In contrast, the proposed method does not depend on the filter configuration and can be implemented in all DQ current controlled schemes without any modifications.

C. Comparison With Stationary Reference Frame Controllers

Superior performance of the proposed method in comparison with several other single-phase DQ frame power controllers has been demonstrated in previous sections. This section aims to compare the proposed method with a stationary reference frame controller. Accordingly, an IPC method [6] is taken into consideration, which directly controls the output power of the single-phase inverter. This method is based on an optimization problem, which provides the control function

$$p^*(t) = P^*(1 + \cos(2\theta)) + Q^* \sin(2\theta) \tag{16}$$

as the reference value of the inverters' instantaneous power. Block diagram of this method is shown in Fig. 12.

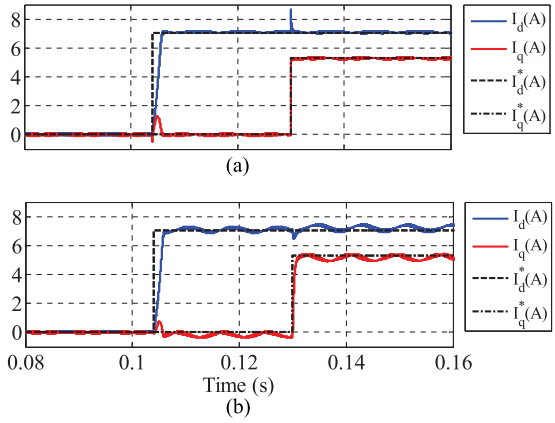

Fig. 10. FAE and the proposed method comparison facing a filter inductor mismatch. (a) Proposed method. (b) FAE method. In this test, P^* changes from zero to 600 W at $t = 0.104$ s and Q^* from zero to 450 VAR at $t = 0.13$ s. Filter inductance is 12 mH while FAE method is implemented with 24-mH value.

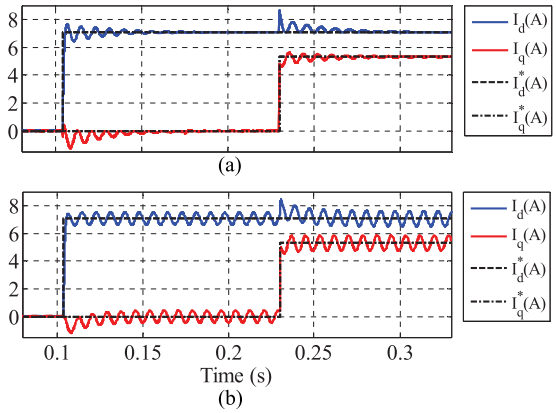

Fig. 11. Dynamic performance evaluation of the proposed and the FAE method for a system using an *LCL* filter. P^* changes from zero to 600 W at $t = 0.104$ s and Q^* from zero to 450 VAR at $t = 0.13$ s. (a) Proposed method. (b) FAE method.

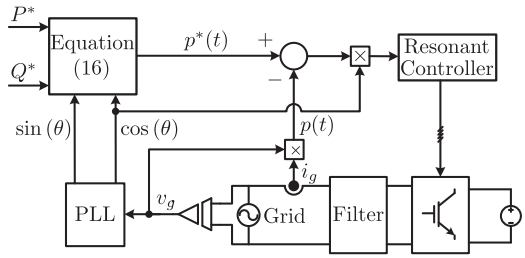

Fig. 12. Block diagram of the instantaneous power controller.

Performance of the proposed method is compared with the IPC method by applying a step change to both active and reactive power reference values. The PR controller for the IPC method is set at $k_p = 0.63$ and $k_r = 0.025$. The resulting grid current waveforms are presented in Fig. 13(a) and (b) showing that both methods are injecting sinusoidal currents to the grid. Furthermore, the reference power tracking performance of these methods are also compared. For this purpose, (16) is taken into account and the error between $p^*(t)$ and instantaneous power value of the inverter (i.e., $p(t) = v_g(t) \times$

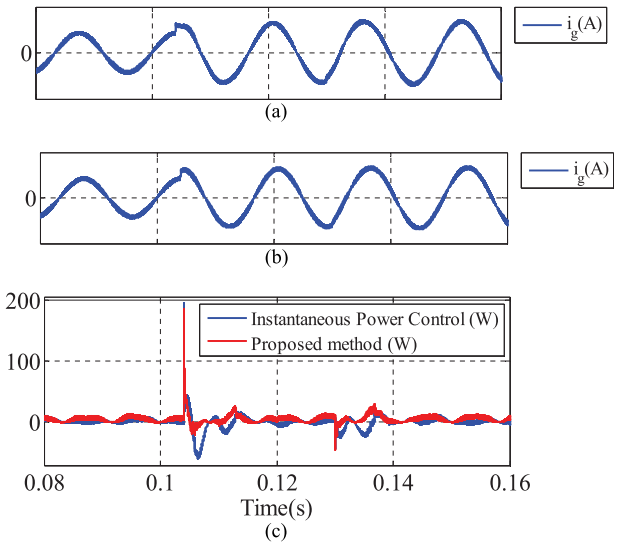

Fig. 13. Proposed method compared with the IPC method. A step change is applied to the active and reactive power set points, at $t = 0.104$ s and $t = 0.13$ s, respectively. (a) Grid current of the system using IPC method. (b) Grid current of the system using the proposed method. (c) Difference between the output power and the reference value for both methods.

$i_g(t)$) is shown in Fig. 13(c). As it can be observed, both methods present perfect power regulation for the inverter, since they are able to track the $p^*(t)$ with fast dynamic and zero steady-state error. As a conclusion, the proposed method provides a power regulation scheme in SRF, which has a competitive performance compared with the advanced stationary frame power controllers.

D. LVRT Performance Evaluation

Performance of the proposed OSG method has been evaluated in LVRT application. German grid code for medium- and high-voltage networks is considered as an example in this section. According to this code, if the grid voltage drops to zero for less than 150 ms, the inverter is required to remain connected to the grid and use all its nominal capacity to provide reactive power for the network [23]. This scenario is simulated and results are shown in Fig. 14. In this test, grid voltage goes from 120 V to zero and vice versa at $t = 0.122$ s and $t = 0.272$ s, respectively. Before the grid outage, P^* equals 600 W and Q^* is zero. As the fault forces the grid voltage to zero, inverter uses all its nominal capacity to generate reactive current to support the grid. When the grid voltage restores, the inverter goes back to its set point values prior to the fault. It can be seen in Fig. 14 that after this outage, PLL provides the synchronization signal very fast, leading to the normal operation of the inverter. Fast dynamic response of the proposed OSG technique allows the control loop to closely follow the reference values of the grid current in both D- and Q-axes.

E. Experimental Results

The proposed method is also experimentally validated. The controller for this laboratory test is implemented in dSPACE DS1104 digital controller setup box. This controller utilizes

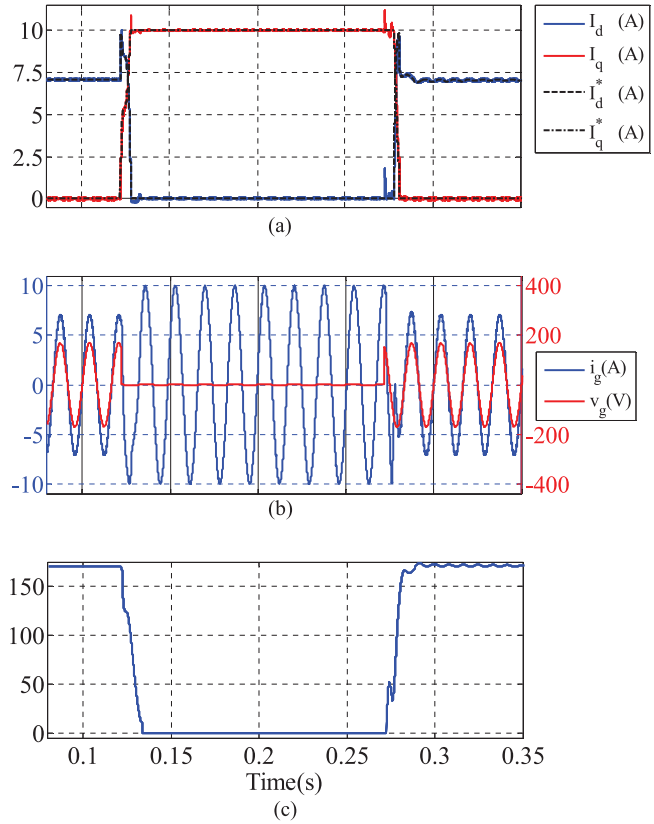

Fig. 14. LVRT performance evaluation. Grid voltage goes from 120 V to zero and vice versa at $t = 0.122$ s and $t = 0.272$ s, respectively. Before and after the grid outage, P^* equals to 600 W and Q^* is zero. (a) Grid current and voltage. (b) Grid current in both D- and Q-axes along with their reference values. (c) Grid voltage amplitude at the PL-EPLL output.

two processors in a master/slave configuration to provide sampling, calculations, and PWM signals for the setup. The dSPACE controller is programmed using MATLAB/Simulink software. Parameters of the system are presented in Table I.

Fig. 15 shows the steady-state and dynamic performance test results. Fig. 15(a) shows the grid current and voltage in steady state. P^* and Q^* are set to 360 W and 180 VAR, respectively. As it can be seen, the inverter injects a high quality sinusoidal current to the grid. In another test, P^* jumps from 45 to 360 W, while Q^* is set to zero. Test result of Fig. 15(b) validates dynamic performance of the proposed method.

Performance of the controller in a distorted grid voltage condition is also experimentally evaluated. In this test, the grid is polluted with 1.5% of the third and fifth harmonic. Fig. 16 shows the result for clean and distorted grid voltage tests. As it can be seen, harmonic contents of the grid current in both cases are within the limits of IEEE 1547 standard. Current THD for nonpolluted and distorted tests are measured as 2.71 and 4.19%, respectively.

In another test, performance of the controller under grid frequency deviations is tested. In this study, the grid frequency jumps from 60 to 60 $\pm$ 5 Hz for 1 s, and then, goes back to the nominal condition. Results are shown in Fig. 17. As it can be seen, the inverter perfectly tracks the frequency change of the

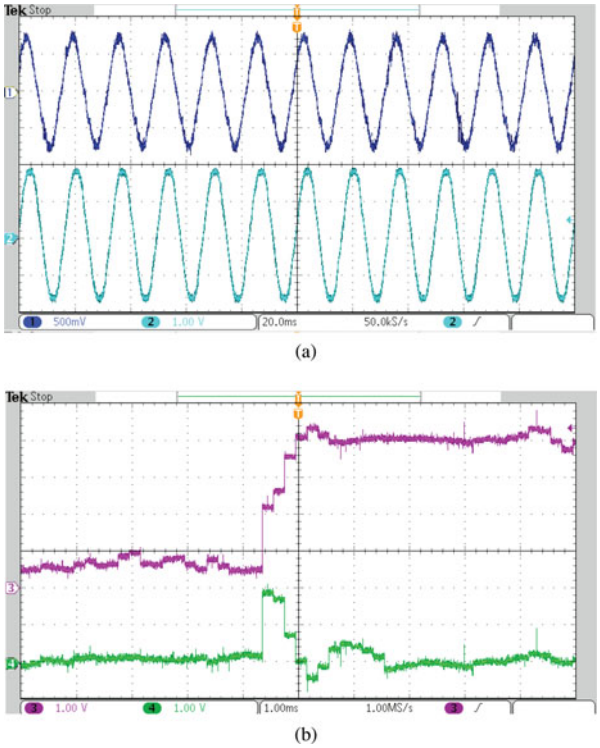

Fig. 15. Experimental results of the proposed technique. (a) Injected current (Ch.1, 3 A/div) and grid voltage (Ch.2, 100 V/div) in steady state. P^* and Q^* are set to 360 W and 180 VAR, respectively. (20 ms/div) (b) I_d (Ch.3, 1 A/div) and I_q (Ch.4, 1 A/div) waveforms during the step change in P^* from 45 to 360 W and Q^* equal zero. (1 ms/div)

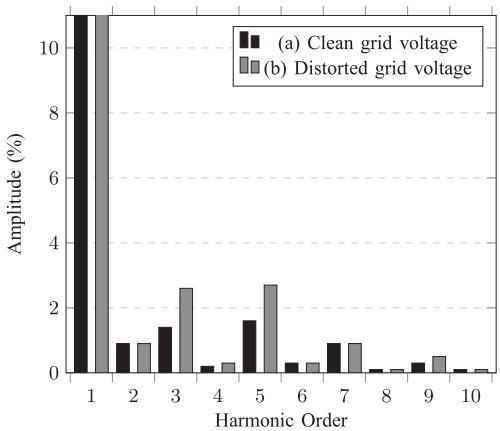

Fig. 16. Experimental harmonic measurement for the grid voltage distortion test. P^* and Q^* are set to 250 W and 0 VAR, respectively. (a) Without harmonics, (b) With 1.5% third and 1.5% fifth harmonic on the grid voltage.

grid voltage and is able to inject the desired power into the grid in nonrated frequencies.

Finally, the proposed approach is evaluated in an LVRT test bench and results are shown in Fig. 18. In this study, the inverter is injecting 170 W and 170 VAR into the grid, when the grid voltage falls to about zero volt for 150 ms. During this grid outage, the inverter goes to LVRT mode of operation and injects reactive current to the grid. Upon restoration of the voltage,

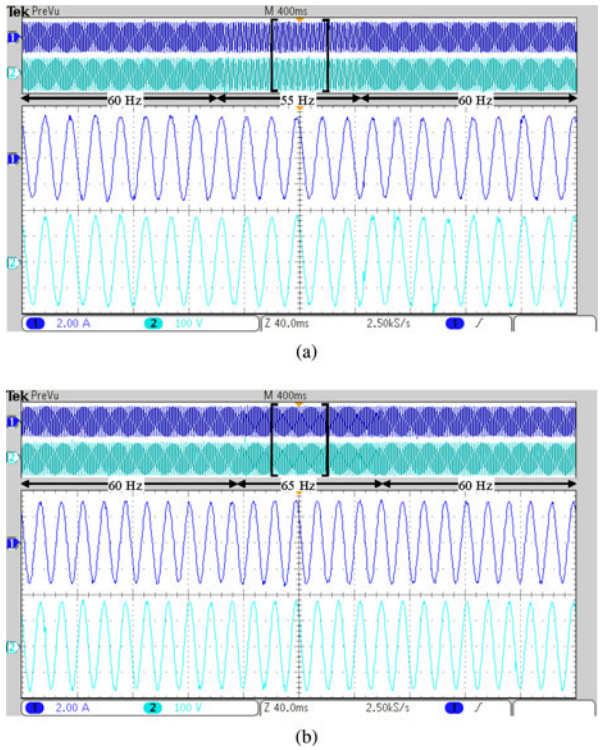

Fig. 17. Grid frequency deviation tests. P^* and Q^* are set to 250 W and 0 VAR, respectively. Ch. 1 shows the grid current (2 A/div) and Ch. 2 is the grid voltage (100 V/div). Top window shows the grid voltage and current (400 ms/div) and a snapshot of the inverter operation during the frequency deviation period is depicted in the bottom window (40 ms/div). (a) 55-Hz test (b) 65-Hz test.

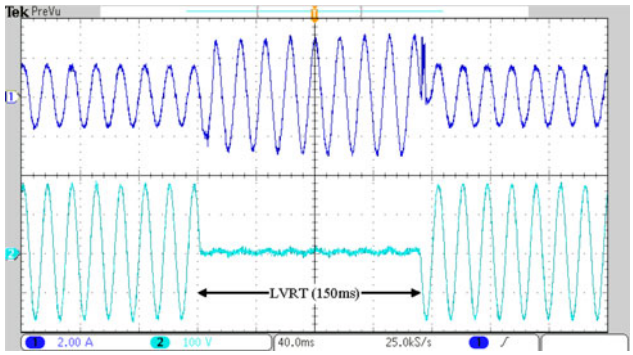

Fig. 18. Experimental result for the LVRT performance. Ch. 1 shows the grid current (2A/div) and Ch. 2 is the grid voltage (100 V/div).

inverter is again synchronized to the grid and goes back to its normal operation prior to the fault.

V. Conclusion

A new OSG technique is introduced in this paper. The proposed method is not based on phase-shift techniques, hence, does not introduce any extra dynamics into the current control loop. It also avoids introducing distortions into the generated orthogonal signal. Feasibility and stability of the proposed method is analytically proved based on the model of the system. Also the system performance has been evaluated by means of simulation and experimental validation. It is shown that this method has

superior dynamic performance in comparison with conventional methods. The proposed method is simulated, implemented and also used to provide LVRT feature for single-phase smart inverters.

REFERENCES

[1] *IEEE Draft Recommended Practice for Establishing Methods and Procedures that Provide Supplemental Support for Implementation Strategies for Expanded use of IEEE standard 1547*, pp. 1–176, Sep. 2014.

[2] *Advanced Functions for DER Inverters Modeled in IEC 61850-90-7*, pp. 1–66, 2012.

[3] EPRI, "Common functions for smart inverters, version 3," Electric Power Research Institute, Palo Alto,CA, USA, 2014.

[4] "California electric rule NO. 21 generating facility interconnections," pp. 1–217, 2015.

[5] California Energy Commission. (2014). Recommendations for updating the technical requirements for inverters in distributed energy resources, pp. 1–91. [Online]. Available: http://www.energy.ca.gov

[6] S. A. Khajehoddin, M. Karimi-Ghartemani, A. Bakhshai, and P. Jain, "A power control method with simple structure and fast dynamic response for single-phase grid-connected DG systems," *IEEE Trans. Power Electron.*, vol. 28, no. 1, pp. 221–233, Jan. 2013.

[7] H. Akagi, Y. Kanazawa, and A. Nabae, "Instantaneous reactive power compensators comprising switching devices without energy storage components," *IEEE Trans. Ind. Appl.*, vol. IA-20, no. 3, pp. 625–630, May 1984.

[8] H. Akagi, E. Watanabe, and M. Aredes, *Instantaneous Power Theory and Applications to Power Conditioning*. New York, NY, USA: Wiley, 2007.

[9] C. Zou, B. Liu, S. Duan, and R. Li, "Stationary frame equivalent model of proportional-integral controller in dq synchronous frame," *IEEE Trans. Power Electron.*, vol. 29, no. 9, pp. 4461–4465, Sep. 2014.

[10] M. Ryan and R. Lorenz, "A synchronous-frame controller for a single-phase sine wave inverter," in *Proc. APEC 97 - Appl. Power Electron. Conf.*, IEEE, vol. 2, 1997, pp. 813–819.

[11] Y. Sozer and D. Torrey, "Modeling and control of utility interactive inverters," *IEEE Trans. Power Electron.*, vol. 24, no. 11, pp. 2475–2483, Nov. 2009.

[12] M. Saito and N. Matsui, "Modeling and control strategy for a single-phase PWM rectifier using a single-phase instantaneous active/reactive power theory," in *Proc. 25th Int. Telecommun. Energy Conf.*, 2003, pp. 573–578.

[13] V. Khadkikar, A. Chandra, and B. Singh, "Generalised single-phase pq theory for active power filtering: Simulation and DSP-based experimental investigation," *IET Power Electron.*, vol. 2, no. 1, pp. 67–78, 2009.

[14] M. Saitou and T. Shimizu, "Generalized theory of instantaneous active and reactive powers in single-phase circuits based on Hilbert transform," in *Proc. IEEE 33rd Annu. Power Electron. Spec. Conf.*, no. 2, 2002, pp. 1419–1424.

[15] S. Dasgupta, S. K. Sahoo, and S. K. Panda, "Single-phase inverter control techniques for interfacing renewable energy sources with microgridPart I: Parallel-connected inverter topology with active and reactive power flow control along with grid current shaping," *IEEE Trans. Power Electron.*, vol. 26, no. 3, pp. 717–731, Mar. 2011.

[16] S. Silva, B. Lopes, B. Cardoso Filho, R. Campana, and W. Boaventura, "Performance evaluation of PLL algorithms for single-phase grid-connected systems," in *Proc. Conf. Rec. IEEE Ind. Appl. Conf.*, vol. 4, 2004, pp. 2259–2263.

[17] R.-Y. Kim, S.-Y. Choi, and I.-Y. Suh, "Instantaneous control of average power for grid tie inverter using single phase DQ rotating frame with all pass filter," in *Proc. IEEE 30th Annu. Conf. Ind. Electron. Soc.*, vol. 1, 2004, pp. 274–279.

[18] J. Choi, Y. Kim, and H. Kim, "Digital PLL control for single-phase photovoltaic system," *Proc. IEE*, vol. 153, no. 1, pp. 40–46, Jan. 2006.

[19] R. I. Bojoi, L. R. Limongi, D. Roiu, and A. Tenconi, "Enhanced power quality control strategy for single-phase inverters in distributed generation systems," *IEEE Trans. Power Electron.*, vol. 26, no. 3, pp. 798–806, Mar. 2011.

[20] B. Bahrani, A. Rufer, S. Kenzelmann, and L. A. Lopes, "Vector control of single-phase voltage-source converters based on fictive-axis emulation," *IEEE Trans. Ind. Appl.*, vol. 47, no. 2, pp. 831–840, Mar./Apr. 2011.

[21] A. Yazdani and R. Iravani, *Voltage-Sourced Converters in Power Systems: Modeling, Control, and Applications*. Hoboken, NJ, USA: Wiley, 2010.

[22] Y. Yang, F. Blaabjerg, and H. Wang, "Low voltage ride-through of single-phase transformerless photovoltaic inverters," *IEEE Trans. Ind. Appl.*, vol. 50, no. 3, pp. 1942–1952, May/Jun. 2014.

[23] Y. Yang, F. Blaabjerg, and Z. Zou, "Benchmarking of grid fault modes in single-phase grid-connected photovoltaic systems," *IEEE Trans. Ind. Appl.*, vol. 49, no. 5, pp. 2167–2176, Sep. 2013.

[24] M. Karimi-Ghartemani and M. R. Iravani, "A nonlinear adaptive filter for online signal analysis in power systems: Applications," *IEEE Trans. Power Del.*, vol. 17, no. 2, pp. 617–622, Apr. 2002.

[25] M. Karimi-Ghartemani, "Linear and pseudolinear enhanced phased-locked loop (EPLL) structures," *IEEE Trans. Ind. Electron.*, vol. 61, no. 3, pp. 1464–1474, Mar. 2014.

Mohammad Ebrahimi (S'11) received the B.Sc. and M.Sc. degrees from the Isfahan University of Technology, Isfahan, Iran, in 2010 and 2013, both in electrical power engineering. He is currently working toward the Ph.D. degree in electrical engineering at the University of Alberta, Edmonton, AB, Canada.

His research interest includes power electronics applications in power and renewable energy systems and high power density converters.

Sayed Ali Khajehoddin (S'04–M'10) received the B.Sc. and M.Sc. degrees in electrical engineering at the Isfahan University of Technology, Isfahan, Iran, and the Ph.D. degree in electrical engineering specialized in power electronics and their applications in renewable energy systems from Queens University, Kingston, ON, Canada, in April 2010.

After completing his Masters, he cofounded a start-up company, which was focused on the development and production of power analyzers and smart metering products used for smart grid applications. During his doctoral research at Queens University, he focused on the design and implementation of compact and durable micro-inverters for photovoltaic (PV) grid connected systems. Based on this research, Queens University spun off SPARQ systems, Inc., where as the lead R&D Engineer, he worked toward mass production and commercialization of microinverters from 2010 to 2013. He joined the Department of Electrical and Computer Engineering, University of Alberta, Edmonton, Canada, in 2013.

Dr. Khajehoddin is an Editor of the IEEE TRANSACTION ON SUSTAINABLE ENERGY and the IEEE CANADIAN JOURNAL OF ELECTRICAL AND COMPUTER ENGINEERING.

Masoud Karimi-Ghartemani (M'01–SM'09) received the Ph.D. degree in electrical engineering from the University of Toronto, Toronto, ON, Canada, in 2004.

He was an Assistant Professor at the Sharif University of Technology, Tehran, Iran, from 2005 to 2008. He worked at the Queens Centre for Energy and Power Electronics Research, Queens University, Kingston, Canada, from 2008 to 2011. He is currently an Associate Professor with the Department of Electrical and Computer Engineering, Mississippi State University, Starkville, MS, USA. His research interests include control of distributed and renewable energy resources, microgrid, power system stability and control, power system measurement, and power quality.